

Title	Enabling landings on irregular surfaces for unmanned aerial vehicles via a novel robotic landing gear
Author(s)	Huang, Tsung Hsuan; Elibol, Armagan; Chong, Nak Young
Citation	Intelligent Service Robotics, 15: 231-243
Issue Date	2022-05-16
Type	Journal Article
Text version	author
URL	http://hdl.handle.net/10119/18320
Rights	This is the author's version of the work. Copyright (C) 2022, Tsung Hsuan Huang, Armagan Elibol, Nak Young Chong, under exclusive licence to Springer-Verlag GmbH Germany, part of Springer Nature. The version published by Springer-Verlag is available at www.springerlink.com , https://link.springer.com/article/10.1007/s11370-022-00420-y
Description	

1 **Enabling Landings on Irregular Surfaces for**
2 **Unmanned Aerial Vehicles via a Novel Robotic**
3 **Landing Gear**

4 **Tsung Hsuan Huang · Armagan Elibol ·**
5 **Nak Young Chong**

6
7 Received: date / Accepted: date

8 **Abstract** Unmanned Aerial Vehicles (UAVs) have been attracting much at-
9 tention and changing our daily lives. Recent technological advances in the de-
10 velopment of UAVs have drastically increased both their general capabilities
11 and areas of application. Among many others, one of the areas that benefits im-
12 mediately from using UAVs could be remote inspection, since they can provide
13 an alternative means of access to structures and collect data from locations
14 difficult to reach for human inspectors. Lately, wall-climbing UAVs outfitted
15 with contact-type sensors have been proposed to collect data for the periodic
16 inspection and maintenance of buildings. However, the major drawback is that
17 they can be used only for flat surfaces. In this paper, we present a lightweight
18 robotic landing gear for enabling UAVs to land on irregular surfaces, without
19 affecting the on-board flight control system that keeps the UAV in level flight
20 during the entire mission. Our novel design uses a vacuum system for robotic
21 landing gear to attach to the surface, and the movable counterweight com-
22 posed of a vacuum motor and other control components to balance the flight.
23 To lighten the total weight of UAV, the proposed robotic landing gear system
24 has only one servo motor for gear operation and a passive mechanical struc-
25 ture that guides the vacuum suction cup at the frontal robotic legs to adapt
26 to different shapes of surfaces. We present details of a prototype mechanism
27 and landing experimental results under different scenarios generated within
28 our laboratory environment.

29 **Keywords** Unmanned Aerial Vehicles · Non-destructive inspection · Landing
30 gear · Vacuum suction · Passive controlled structural mechanism

31 **Mathematics Subject Classification (2020)** 70B15 · 70E60

All authors are with the School of Information Science, Japan Advanced Institute of Science and Technology, Nomi, Ishikawa 923-1292, Japan. E-mail: {s2010063, aelibol, naky-oung}@jaist.ac.jp

1 Introduction

Nowadays robotic vehicles are increasingly used in a variety of applications and changing our daily life. With the improvements in their capabilities (*e.g.*, mobility, exploration, data collection, autonomy, and many others), they have been viable for the tasks that need to take place in hazardous environments. Periodic maintenance and inspection of man-made high-rise structures is one of such tasks. It is widely known that Wall Climbing Robots (WCRs) were proposed to use for inspection and cleaning of buildings, replacing long reach fixed based manipulators. However, the moving speed of WCRs is usually relatively slow, which often needs to be provided by roof cables and winches. This significantly limits the scope of applications of WCRs. Notably, the Unmanned Aerial Vehicle (UAV) technology has made astonishing progress in recent years, and its application areas are not only limited to aerial photography, entertainment, and similar others. An increasing number of tasks requiring UAVs to physically interact with their surroundings have been demonstrated (*e.g.*, inspection [17, 8] and agriculture [12, 6, 5]). In light of recent technological advances of UAVs in payload capacity, endurance, flight stability and control, and user interface, as well as the decline in the price of hardware platform, UAVs begin to be used for civil operations under the related regulations and guidance. Therefore, UAVs are deemed as an appropriate alternative for the maintenance and inspection tasks to overcome the aforementioned issues with WCRs. For this reason, we propose a lightweight robotic landing gear prototype that enables the UAV to attach ideally to any shape of the surface.

Different application-oriented platforms [22, 13] have been developed in response to the nature and needs of bridge inspection tasks. As mentioned above, off-the-shelf or custom-built UAV platforms can be potentially utilized for non-destructive inspection and maintenance of man-made high-rise structures, bridges, and bodies of airplanes. There have already been several attempts in remote inspection (*e.g.*, wall, dam, and many others [23, 25]), in which UAVs were an indispensable tool thanks to their ability to obtain data through optical sensors available on board. Specifically, for non-destructive inspection on high-rise buildings, there is always the risk of being affected by the wind. Therefore, it is of utmost importance to keep the UAV attached to the target surface securely and obtain the necessary data correctly.

This paper proposes a novel robotic landing gear for off-the-shelf UAVs, which aims to enable it to land on any shape of surfaces. This design uses only one servo motor to reduce weight and power consumption, combined with a universal joint and multi-link design to achieve a high level of efficiency in irregular surface landing. This robotic landing gear with a mechanical structure weighs less than 1 kilogram. Using only one servo motor and two vacuum motors can allow a UAV to land on different shapes of surfaces. In general, if mobile robots should be endowed with the capability of performing a large set of movements, it means that multiple motors are incorporated into the drive mechanism, which will cause an increases in total power consumption and weight. In order to keep the weight a minimum, we have adopted passive

77 mechanical structures, minimizing the number of motors while keeping the
78 expected function unaffected. This makes it possible for a UAV outfitted with
79 the proposed landing gear to access complex and dangerous environments, such
80 as industrial facilities, disaster sites after earthquakes, and similar others, and
81 collect data in an energy-efficient manner.

82 The rest of the paper is organized as follows. Section 2 briefly overviews
83 the existing designs that enable UAVs to perform some tasks on surfaces.
84 Section 3 presents our proposed landing gear in detail. In Section 4, we present
85 our findings derived from a series of experiments on different surface landing.
86 The last section is devoted to draw conclusions and suggest future research
87 directions.

88 2 Related Work

89 Remote inspection and maintenance is one of the important areas in which
90 robotic platforms can be used intensively. For example, mobile robots can
91 provide a viable solution in the infrastructure inspection sector, since they can
92 move or even fly over vertical and sloped surfaces to reach high-risk locations in
93 civil structures [3]. Specifically, WCRs are a specialized kind of mobile robots
94 potentially used in periodic inspections and maintenance [4]. WCRs may have
95 higher payload carrying capability and better endurance. However, they are
96 usually unwieldy and apply a lower speed limit. Therefore, in recent years,
97 many wall-climbing UAVs have gradually replaced WCRs in bridge inspections
98 and other high-altitude tasks [24, 1].

99 A variant of WCR based on the UAV platform is called as PRWCR (Propeller-
100 type Wall-Climbing Robot) [16]. Several different methods for attaching to
101 the target surface have been proposed such as micro-spine [21], manipula-
102 tor [9], vacuum system [26], and the power of UAV itself [19]. The feature,
103 advantages, and disadvantages of various designs are briefly summarized in
104 Table 1. PRWCRs are used instead of conventional UAVs, since many tasks
105 such as cleaning or inspection require secure contact with the target surface.
106 However, the existing PRWCRs are often designed and developed for applica-
107 tions on vertical walls and usually cannot be used on discontinuous or irregular
108 surfaces effectively, which still limits the usages of UAVs on such robots. In
109 order to endow off-the-shelf UAVs with the capability of landing on arbitrarily
110 shaped surfaces, a viable solution is the development of a landing gear mounted
111 underneath a UAV that can adapt to complex landing surface conditions. It
112 is highly desirable due to the limited battery capacity that the landing gear
113 configuration be controlled by a small number of motors, without affecting
114 the flight control system or requiring a sophisticated flight control during the
115 entire mission.

116 In [17], Myeong *et al.* added an additional structure to the UAV. To effec-
117 tively use the thrust force of the UAV, they control the structure to adjust the
118 angle between the UAV and the wall. However, the purpose of this work is to
119 make the UAV attach to the wall instead of landing. Therefore, this design can

neither turn off the power of the UAV nor fixed at the same position for a long time. In [21], a UAV capable of perching and climbing with passive technology was proposed through the cooperative robotic platform with a 2 degrees-of-freedom climbing mechanism. Although their platform was lightweight and could perch on rough exterior surfaces, it was not able to adapt to uneven surfaces. Furthermore, the payload was also comparatively low for installing additional sensors and/or other equipment for different tasks. In contrast, our design attempts to use a set of vacuum suction cups as an alternative to the aforementioned climbing mechanism. This makes the platform secure a better payload capability, more stable on the surface, and more powerful to perch on the surface. For irregular surfaces landing, Paul *et al.* proposed a UAV equipped with 3 manipulators [20]. This design can effectively land on irregular surfaces. After sensing the shape of the target surface through the sensor, the joints of each manipulator are set to fit the target surface. However, this design still has limitations on the landing angle, and it cannot land on an inclined plane above 40° including perpendicular surfaces. And in [15], Kamel *et al.* presented a mechanical design of UAV platform with a tiltable rotor. They demonstrated a transition from horizontal to upside flight and physical interaction with a wall. Their design is limited to land only on the planar surface. This way of design using the tiltable rotor technology might not be entirely feasible to land on irregular surfaces and the tiltable rotor also could experience a speed problem of slow rotor tilting. Also, maneuverability has become harder than conventional UAVs and it requires a higher battery power.

In [2], in order to make the UAV land on an inclined surface, Bass *et al.* proposed to use the reverse thrust of UAV to extend the landing slope, and it can nearly double the maximum inclination. Although the ability of the bidirectional rotor alone can make the UAV land on the inclined surface, for larger inclination angles and more complex real-world environments, it still needs to be completed with the lightweight robotic landing gear.

Table 1 A comparison of existing surface attaching systems for UAVs

Design	Feature	Advantage	Disadvantage
[21]	micro spines (Landing)	UAV stops when landed Efficient battery usage	No landing on irregular surfaces Limited payload due to micro spines
[11] [18] [27]	wheels (Attaching)	Mobility on the surface agile than wall-climbing	Difficult to be kept at a fixed position
[7] [9] [10]	manipulators (Attaching)	Accurate attaching position using contact-type sensors	Mobility difficulty on irregular surfaces Balance issues due to the arm length
[14] [19]	UAV itself (Attaching)	No extra mechanism needed	Difficult to attach to irregular surfaces and install with contact-type sensors

148

3 Novel Design for Robotic Landing Gear

149

In this section, we provide details on the proposed robotic landing gear for off-the-shelf UAVs made up of 3 different parts; the Angle Control Part (ACP),

150
151

152 the Counterweight Control Part (CCP), and the Environmental Sensor Part
153 (ESP). As a part of its modular design, the distance between the front leg
154 and the rear leg can be adjusted according to users' needs and the size of the
155 UAV. Specifically, responding to the mass distribution changes and the center
156 of mass shifts, only the location of CCP needs to be adjusted backwards and
157 forwards with respect to the servo motor position of the front leg prior to take-
158 off. This will allow the proposed landing gear to accommodate different-sized
159 UAVs without any adverse impact on its landing capability. The type of UAV
160 used is based on the DJI F450 frame with a brushless motor of 14.8V/9.5A-
161 920rpm/V. It has a very limited payload of $1kg$. The motivation behind using
162 the UAV with such a low payload is to enforce our design as minimum as
163 possible so that it can be used by any type of UAV with a payload capacity
164 of more than $1kg$. The proposed robotic landing gear weighs only $900g$. The
165 installation of these parts is shown in Fig. 1. The robotic legs are designed
166 to be attached to the surface with a vacuum system. The CCP is composed
167 of the rather heavy and essential parts; a vacuum motor and a battery. Since
168 the landing gear is mounted underneath the UAV, the weight reduction and
169 the center of gravity change adjustment become particularly important. De-
170 pending on both payload and size of the UAV, the position of the CCP can
171 be adjusted manually when the landing gear is being attached to the UAV in
172 such a way that it keeps the center of gravity of the UAV with the landing
173 gear as close as possible to the center of the original UAV. The ESP is the
174 place to install various types of sensors for intended applications (*e.g.*, RGB-D
175 camera, Lidar, Heading, IMU, and related others) in order to sense the target
176 landing surface details, including the titling angle of the wall relative to the
177 UAV approaching direction. In this paper, we focus on the ACP and mechan-
178 ical structure design of the landing gear. The ACP consists of a servo motor
179 with $25kgf \cdot cm$ torque, two front robotic legs, and a non-slip leg. This design
180 is inspired by the triangular landing gear designs used in commercial aircraft
181 systems. Such triangular systems have been referred to as the most stable poly-
182 gons. Two vacuum suction cups are mainly designed as a backup/emergency
183 plan for any failure that might appear during landing and/or attaching to the
184 surface. The CAD model of the prototype is shown in Fig. 2.

185 To better understand how the robotic landing gear can land on different
186 shapes and inclinations of surfaces, we define the target surface in the world
187 coordinate system (or the XYZ Cartesian axes) separately in the XY and XZ
188 plane as illustrated in Fig. 3. While the robotic leg in the front accommodates
189 the difference in surface shapes in the XZ plane, the front leg and the rear
190 non-slip leg forms a closed-chain structure by attaching to the surface in the
191 XY plane.

192 3.1 Design of the Robotic Legs

193 Each robotic leg has a vacuum suction cup with a $60mm$ diameter, a set
194 of universal joints, a compression spring, and a vacuum tube. Each suction

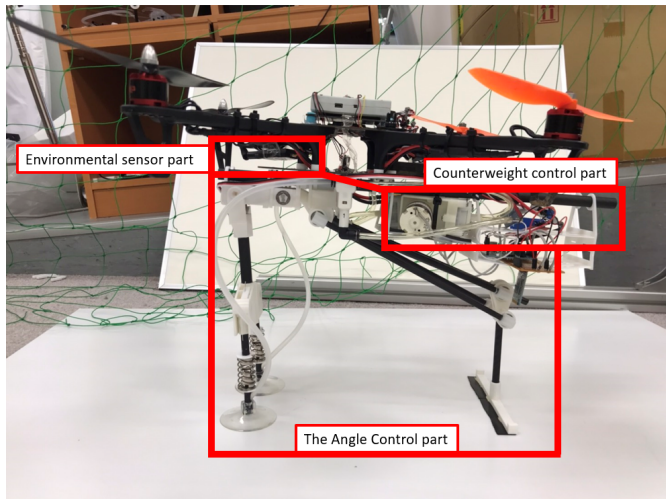


Fig. 1 Installation positions of angle control, counterweight, and sensor parts.

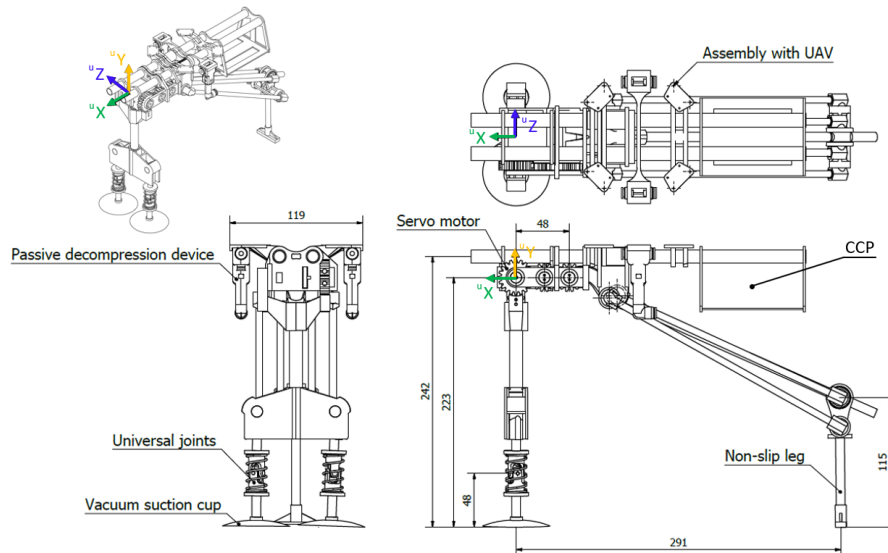


Fig. 2 The CAD drawing of the robotic landing gear. A servo motor controls the angle between the front leg and uX axis of the UAV.

195 cup can generate a suction force of $37.68N$ collocation with a DC $12V/0.4A$
 196 vacuum motor. The suction mechanism can withstand a maximum load of
 197 $10kg$ under the 3D printing parameters (e.g., density, infill, the material used,
 198 and similar other parameters) we used. For different angles of inclination of
 199 landing surface, robotic legs work passively on adjusting the vacuum suction
 200 cup's angle when contacting the surface as shown in Fig. 4 automatically.

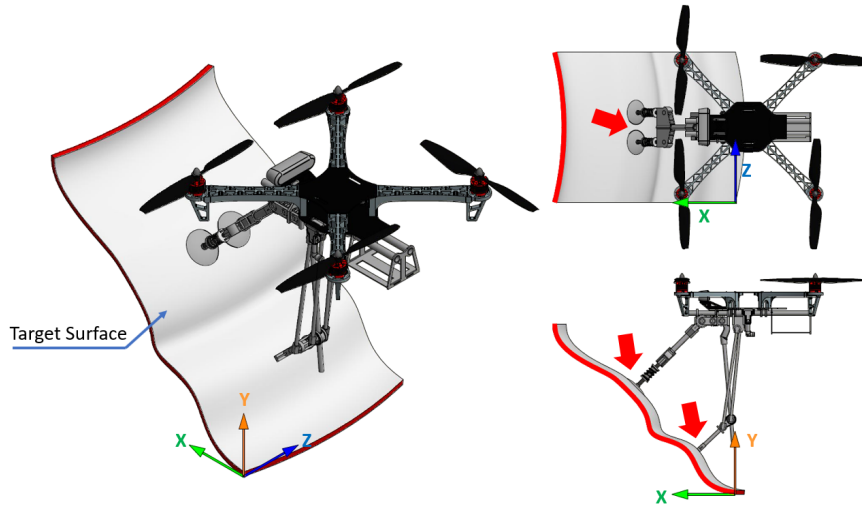


Fig. 3 The projection of a 3D surface onto the XZ and XY planes. The varying surface curvature appears as a curved line, such as the red line in the figure, from which the shape of surface can be coarsely defined. Using this line, the landing gear is set up to its landing configuration.

201 Since the robotic landing gear uses a vacuum system to keep the UAV
 202 attached to the surface, the vacuum suction cup must be perpendicular to the
 203 target surface to maximize the adhesive force. In order to adapt to the different
 204 shapes of the surface, this design allows the robotic leg to be kept perpendicular
 205 adaptively to the surface and attached to it. Moreover, it can also correct slight
 206 angle errors when landing. In terms of structural design, the universal joint can
 207 provide the vacuum suction cup with about 45° of steering in all directions. The
 208 steering degree of the universal joint is based on the shape of the target landing
 209 surface and the velocity of the UAV when approaching the target surface. The
 210 greater the velocity, the greater the rotation angle of the universal joint due
 211 to the compression spring used. The analysis of usable steering angle of the
 212 actual universal joint will be presented in the Experimental Results section.
 213 When the UAV needs to leave the target surface, the compression spring will
 214 return the vacuum suction cup to the original position for the next landing.

215 The two robotic legs in the front are separated into two sides using a torsion
 216 spring to keep them parallel. In this way, we can enable the robotic landing
 217 gear to land on different shapes of surface and achieve the cushioning effect
 218 by absorbing the shock during UAV landing. Even though the surface is not
 219 purely planar in the XZ plane, the torsion spring and the universal joint are
 220 flexible enough to accommodate different shapes of the surface. Some examples
 221 are shown in Fig. 5.

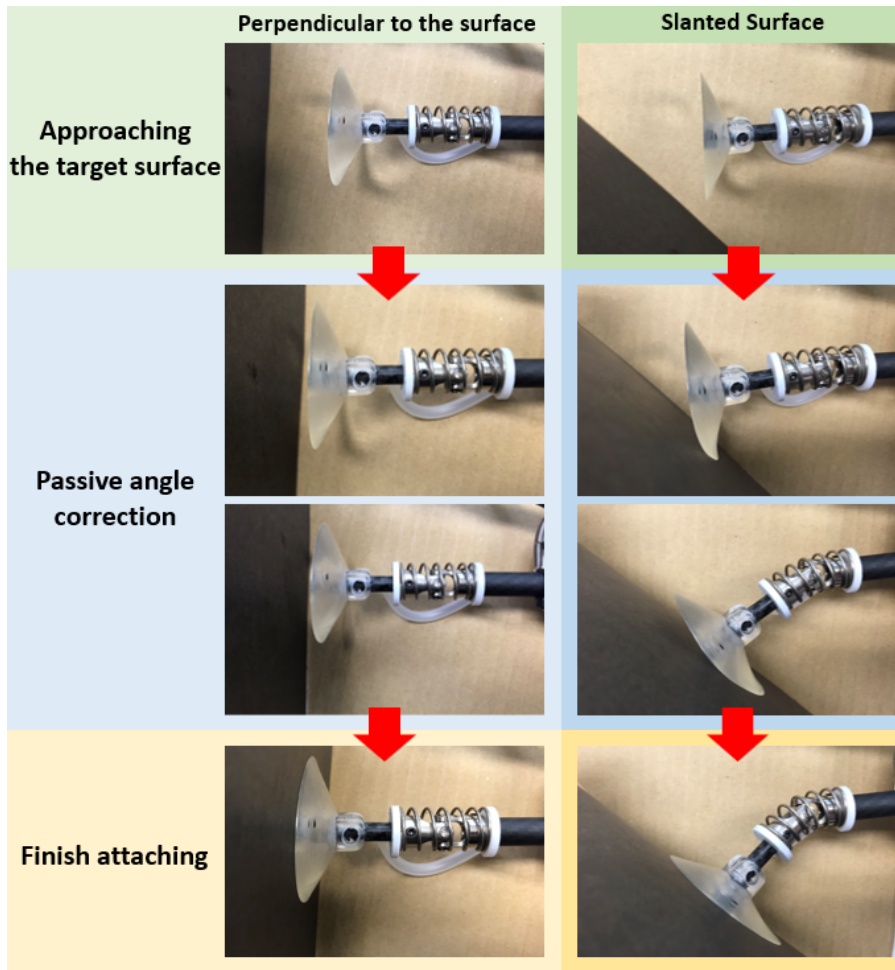


Fig. 4 Attaching to the target surface: When the soft rubber part of the vacuum suction cup touches the landing surface, the friction between the rubber and the surface will steer the universal joint, keeping the vacuum suction cup perpendicular to the surface.

222 3.2 Structure of the Front and Rear Legs Part

223 The mechanical structure of the front leg and the rear leg adapt to the surface
 224 in the XY plane. Since a single motor controls the angles of the front and
 225 rear leg configurations in ACP, in order to keep both legs parallel to the
 226 landing surface, we need to determine a gear ratio to make the non-slip rear
 227 leg rotate more than the front leg. Using the linkage method of multiple rods,
 228 the non-slip leg can change the angle and length with only a single motor input
 229 simultaneously. This design can make the front and rear legs have different
 230 angle changes, enabling them to adapt to the surface of different curvatures.
 231 Since the robotic landing gear uses a vacuum system to keep the UAV attached

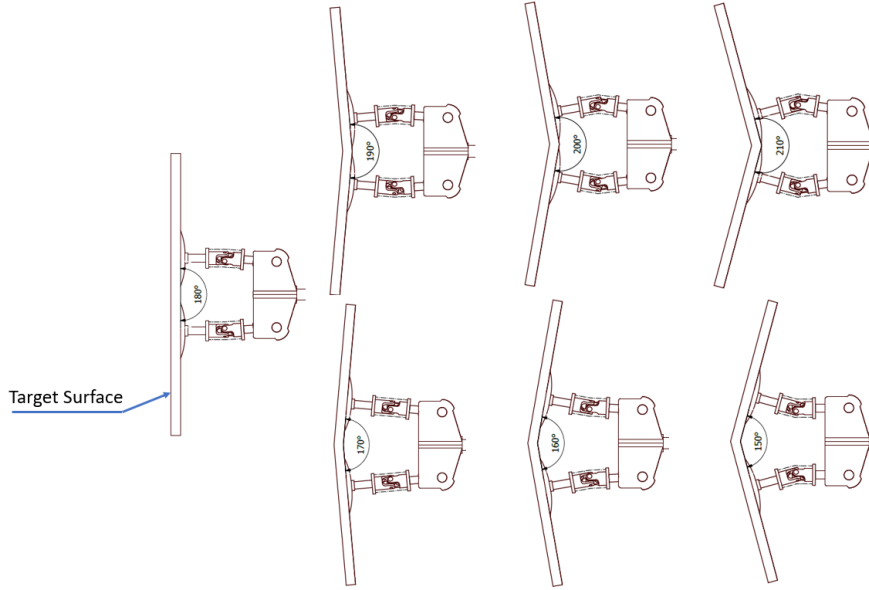


Fig. 5 The two front robotic legs are flexible enough to accommodate any shape in the XZ plane. The back leg is only to support the entire landing gear, therefore it will not affect the difference in the XZ plane.

232 to the surface, it is important to ensure that the legs of the landing gear are
 233 perpendicular to the target surface. We define the ground plane as an angle of
 234 0° surface, and a vertical plane perpendicular to the ground as an angle of 90°
 235 surface. Our novel design structure can make the landing gear land between
 236 0° and 100° . Regardless of any angle of inclination of the target surface, it can
 237 keep the 3 legs perpendicular to the target surface.

238 We assume that the angle of inclination of the target surface is α , Θ_1 is
 239 the angle controlled by the servo motor, Θ_2 is the angular position of the rear
 240 leg, and Θ_3 is the rotation angle of the rear leg to the surface. For the cases
 241 where $\Theta_1 \in (0, \pi/2]$, we can make use of triangular representations as shown
 242 in Fig. 6. Then the angular relationship between the target surface and the
 243 servo motor (front leg) is given by

$$\alpha + \Theta_1 = \frac{\pi}{2}. \quad (1)$$

244 The front leg and the rear leg are driven by a gear with a ratio of 1 :
 245 1.28. This ratio is derived from the data obtained from simulations in the
 246 AutoDesk Inventor environment by modeling a linear relationship between Θ_2
 247 and Θ_1 . Therefore, the angle relationship between the front and the back leg
 248 is described by

$$\dot{\Theta}_2 = 1.28 \times \dot{\Theta}_1. \quad (2)$$

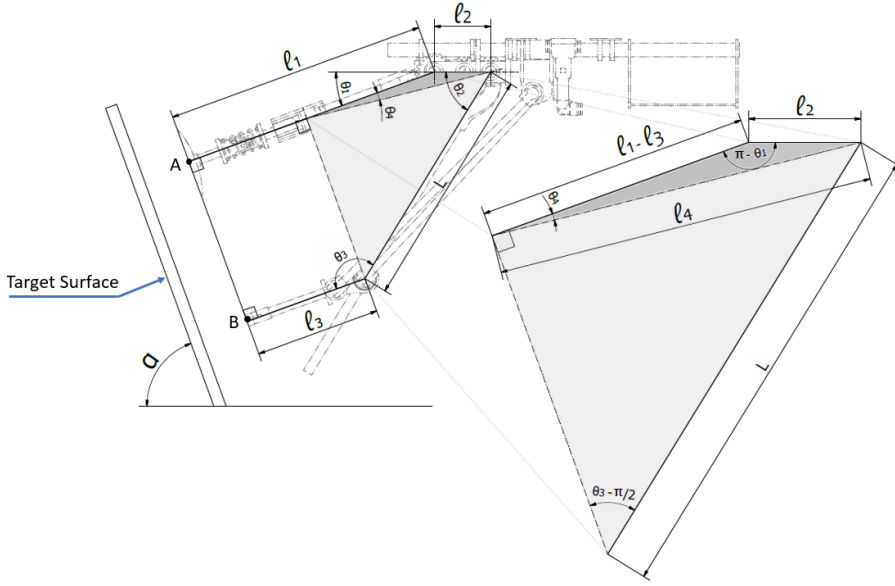


Fig. 6 This figure is the setup of landing gear for an example of the $\alpha = 70$ degree target plane. It shows the definition and position of each angle within the main structure.

249 From the entire structure of the polygon with $n = 5$ sides, by using the
 250 formula for the sum of the interior angles $(n - 2) \times \pi$, the relationship between
 251 the Θ_3 and other angles can be written as follows:

$$\begin{aligned} \frac{\pi}{2} + \frac{\pi}{2} + \Theta_3 + \Theta_2 + \pi - \Theta_1 &= (5 - 2) \times \pi \\ \Theta_3 + \Theta_2 - \Theta_1 &= \pi \end{aligned} \quad (3)$$

252 With different surface inclination angles, the angle Θ_1 (thus, Θ_2 and Θ_3)
 253 and length L will change at the same time accordingly. To calculate the length
 254 L , we can first calculate l_4 using the law of cosines in the dark gray triangle
 255 in Fig. 6.

$$\begin{aligned} l_4^2 &= (l_1 - l_3)^2 + l_2^2 - 2l_2(l_1 - l_3) \cos(\pi - \Theta_1) \\ &= (l_1 - l_3)^2 + l_2^2 + 2l_2(l_1 - l_3) \cos(\Theta_1) \end{aligned} \quad (4)$$

256 where l_1 , l_2 , and l_3 are leg segment lengths. After computing l_4 , by using the
 257 law of sines, Θ_4 can be calculated as follows:

$$\begin{aligned} \frac{l_2}{\sin \Theta_4} &= \frac{l_4}{\sin(\pi - \Theta_1)} \\ \Theta_4 &= \sin^{-1} \left(\frac{l_2 \sin \Theta_1}{l_4} \right) \end{aligned} \quad (5)$$

258 After calculating ℓ_4 and Θ_4 , from the bigger triangle (colored light gray in
259 Fig. 6), the length L can be calculated using the law of sines given by

$$\begin{aligned} \frac{L}{\sin(\frac{\pi}{2} - \Theta_4)} &= \frac{\ell_4}{\sin(\Theta_3 - \frac{\pi}{2})}, \\ L &= \frac{\ell_4 \cos \Theta_4}{-\cos \Theta_3}. \end{aligned} \quad (6)$$

260 With this design, for the surface in the XY plane to which the front and
261 rear leg are positioned, any shape of the surface can be regarded as a plane
262 with a different angle of inclination. The angle α with the ground plane can be
263 calculated via a line segment connecting the landing points. Then Θ_1 can be
264 set in such a way to keep the front and rear leg parallel to the landing surface.
265 The universal joint at the front end of the robotic leg can passively perform
266 a slight angle correction, according to the actual shape of the surface at the
267 landing point. However, instead of using a robotic leg with a vacuum suction
268 cup, the rear leg is designed to be a non-slip leg. From our experiments, it was
269 noticed that when all the legs in contact with the target surface are equipped
270 with universal joints, the structural rigidity is seriously insufficient and it could
271 cause the landing gear to fall off the target surface easily. It would also cause
272 the UAV to be unable to land in a horizontal attitude after the power is
273 turned off. Also, when leaving the target surface, it could lead to a control
274 loss when the UAV propellers start to rotate again. It also limits the types of
275 target surfaces. For discontinuous surfaces, the success rate of landing would
276 decrease due to insufficient rigidity. The advantages of designing the rear leg
277 with a non-slip foot is not only to solve the aforementioned issues, but also
278 not to affect the adsorption force of the vacuum system on the target surface.
279 It has also a better landing effect for discontinuous surfaces.

280 3.3 Design of the Passive Decompression Device

281 When the UAV needs to leave the surface, the vacuum system needs to be
282 decompressed to release the vacuum environment so that the UAV can take
283 off smoothly. For this reason, we design a passive decompression device as
284 shown in Fig. 7. Compared to the electronic decompression device, the passive
285 decompression device is lighter and less power-demanding, while preserving
286 the necessary functionality. This passive decompression device is composed of
287 three parts: the air intake part, the outtake part, and air disperse housing. The
288 air intake part is connected to the air disperse housing, the vacuum suction
289 cup, and the air inlet part of the vacuum motor. The air outtake part is
290 connected to the air disperse housing and the air outlet part of the vacuum
291 motor. The air disperse housing connects the intake part and outtake part,
292 and has a small steel ball in the center.

293 The outtake part will blow the small steel ball upward when the vacuum
294 motor is turned on. Since the vacuum suction cup has not been attached to

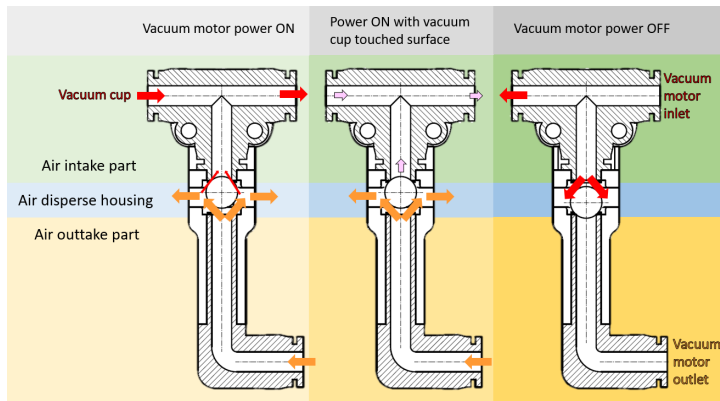


Fig. 7 When the vacuum motor is turned on, the small steel ball is blown upward by the air from the outtake part and blocks the intake part. Since this air intake part is connected in parallel with the vacuum suction cup, the small steel ball will not be fully blocking the air intake part until the vacuum suction cup is attached to the surface.

295 the target surface, the intake part will not become in a negative pressure state.
 296 Therefore, the part sucking the small steel ball has almost no suction for the
 297 small steel ball. This is because the vacuum suction cup and the sucking part
 298 are connected in parallel within the intake part. Therefore, until the vacuum
 299 suction cup is attached to the target surface, it will increase the suction power
 300 of the part that sucks the small steel ball and blocks it. And the intake part
 301 will be in negative pressure state to complete the suction step. When the UAV
 302 needs to leave the surface, it is only necessary to stop the vacuum motor. The
 303 small steel ball will quickly leave the air intake part, opening (the previously
 304 closed) air intake part. By doing so, the vacuum suction cup can be removed
 305 from the surface smoothly and quickly. While a small vacuum solenoid valve
 306 weighs around 50 grams, this passive pressure reduction unit weighs only 9
 307 grams. Since every extra weight means more power consumption for the motor
 308 of UAVs, we opted to use a passive pressure-reducing device in order to keep
 309 the proposed robot landing gear as light as possible. The passive pressure-
 310 reducing device not only requires no additional control but also is lighter.

311 3.4 The Operational Principle of Robotic Landing Gear

312 A brief operation process is given in Fig. 8. Right after takeoff, the ACP rotates
 313 the robotic legs up and makes them face front (the direction of flight) and keeps
 314 them horizontal. When approaching the target surface, the 3D shape of the
 315 surface is detected using the data provided by the sensor part and set up the
 316 robotic legs adjustments accordingly to start the vacuum system and be ready
 317 to approach the target surface. The decision of whether the robotic legs are
 318 fully attached to the surface or not is determined via the vacuum value. When

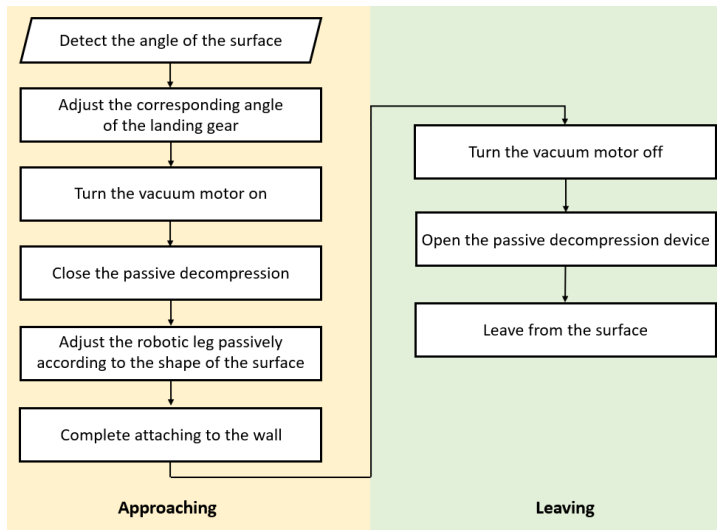


Fig. 8 A brief operation process of the landing gear divided into two parts: approaching and leaving. After leaving the current surface, return to the approaching part for next target surface landing.

319 taking off the surface again, the vacuum system is turned off and the power
 320 of the UAV is throttled to leave the surface.

321 4 Experimental Results

322 We carried out a preliminary landing experiment with an in-house built terrain
 323 generation system as shown in Fig. 9. This testbed allows creating different
 324 undulating surfaces by adjusting the angle of the landing plane. We also adjust
 325 test surfaces by calculating the distance between the front and rear legs. The
 326 limit curvature radius (R) of the surface can be calculated by using the angles
 327 (θ_{FR} , θ_{FL} , θ_{Back}) and the distance (D).

328 During the experiments, we attached the robotic landing gear to a custom-
 329 built quadcopter based on commercially available DJI F450. After experiment-
 330 ing with various landing trials (10 for each angle combination), the success
 331 rate of the robotic landing gear for different types of surfaces is presented in
 332 Table 2. The first two columns denote the angle configurations used in the
 333 landing terrain testbed, referring to Fig. 9, while the third column represents
 334 the contact area between the non-slip leg and the surface being tested. As a
 335 result of experimental tests, the landing limits for the robot were within 50°
 336 of the tangent point of the irregular surface and $R \geq 200mm$ obtained by
 337 the geometrical relation $D = 2 \times R \times \sin(\theta)$. D changes depending on the
 338 UAV size and also the small variation caused by passive joints (see Fig. 4 and
 339 Fig. 12). In our case, D was approximately $300mm$. During the experiments,
 340 failed landing attempts have been observed when the tilt angles of both the

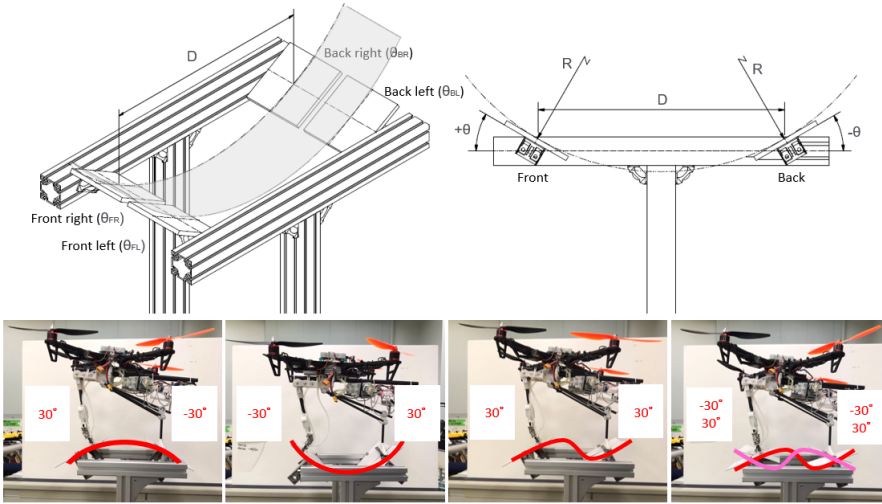


Fig. 9 The uneven landing terrain testbed to simulate different types of surfaces by changing the surface undulation angle. We define the angle change in clockwise direction as positive and counterclockwise as negative.

341 front and back planes are very large and in the same direction. The reason is
 342 the lack of enough friction force generated by the vacuum cup material. That
 343 leads to making it difficult to guide the universal joint when it touches the
 344 landing surface. It was observed from the experiments that the rear non-slip
 345 leg design was able to land successfully regardless of the landing surface angle
 346 variations and unevenness of the landing surface.

347 We then proceed to the main experiments covering the entire flight and
 348 landing process. In our experiments, we use 6 different types of surfaces with
 349 smooth material (*e.g.*, plastics and metals) as shown in Fig. 10, including a
 350 vertical surface, a 45-degree slope surface, a discontinuous surface with eleva-
 351 tion differences, and 3 types of curved surfaces with various radii of curvature,
 352 to test whether the robotic landing gear can successfully land on uneven sur-
 353 faces. The whole operation process is divided into several steps: taking off,
 354 setting robotic legs to the initial position (defined by $\Theta_1 = 0$), approaching
 355 target surface, contacting target surface, and decreasing power. The overall
 356 pipeline of the experiment is given in Fig. 11.

357 We measured the Θ_3 and L distance during the landing experiments on
 358 different angled surfaces. We also computed the same values using Eqs. (1)-
 359 (6) and obtained values are given in Fig. 12. Some small error can be seen
 360 between values and this is mainly the right angle assumption between legs
 361 and the surface contact points. These errors are mostly compensated by the
 362 universal joints of front legs, demonstrating their importance in the proposed
 363 design. Since universal joints can compensate for some deviations from the
 364 right angle, the legs are not necessarily perpendicular to the surface all the
 365 time.

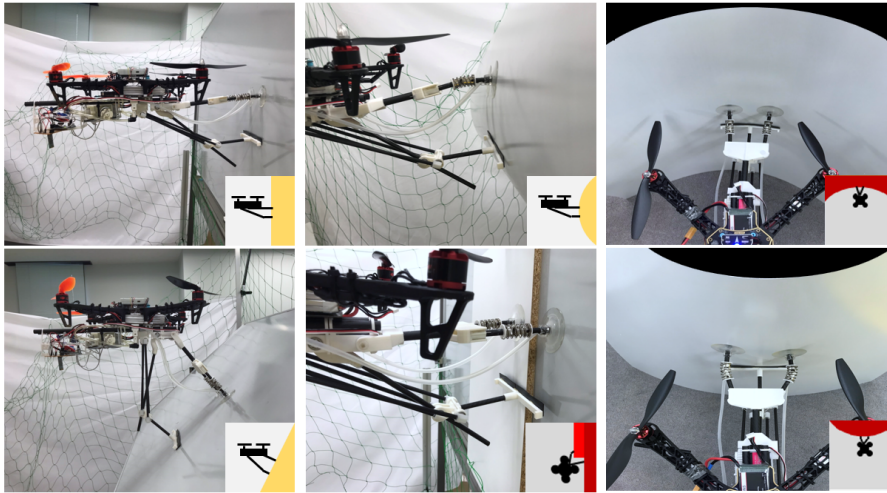


Fig. 10 Some examples of landing on arbitrarily shaped surfaces. The landing gear can easily connect to a variety of surfaces with different curvatures through passive universal joints.

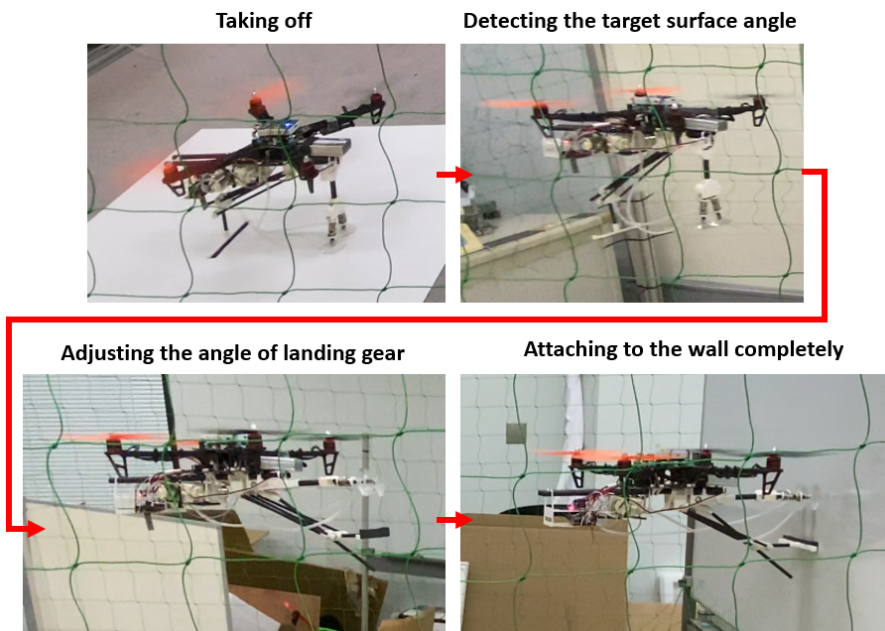


Fig. 11 The figure shows the operational principle of robotic landing gear. According to the calculation of the center of gravity of the entire UAV system, given the counterweight position pre-adjusted while the robotic landing gear was being attached to the UAV, the angle of the robotic legs changes during the flight without affecting the flight stability and balance control. A sample flight scenario can be seen at <https://youtu.be/fbsFB1-dzFs>.

Table 2 Success rate experimental trials for different type of surface

$\Theta_{FL} = \Theta_{FR}$ in degrees	$\Theta_{BL} = \Theta_{BR}$ in degrees	Contact area of non-slip leg	Success rate
0	0	full	100%
10	10	full	100%
20	20	full	100%
30	30	full	100%
40	40	full	70%
50	50	full	50%
10	-10	full	100%
20	-20	full	100%
30	-30	full	100%
40	-40	full	80%
50	-50	full	70%
-10	10	full	100%
-20	20	full	100%
-30	30	full	100%
-40	40	full	80%
-50	50	full	80%
-10	-10	full	100%
-20	-20	full	100%
-30	-30	full	100%
-40	-40	full	60%
-50	-50	full	50%

Θ_{FL}	Θ_{FR}	Θ_{BL}	Θ_{BR}	Contact area of non-slip leg	Success rate
-10	10	-10	10	full	100%
-20	20	-20	20	full	100%
-30	30	-30	30	full	100%
-40	40	-40	40	full	60%
-50	50	-50	50	full	70%
-10	10	-10	10	half	100%
-20	20	-20	20	half	100%
-30	30	-30	30	half	100%
-40	40	-40	40	half	60%
-50	50	-50	50	half	60%

366 In order to make the universal joint automatically return to its original
367 position, we use springs to perform the task of passive return. Among the
368 ones we tested, we found that $\emptyset 1.4 \times 19 \times 55$ and $\emptyset 1.2 \times 20 \times 40$ were too soft,
369 while $\emptyset 1.6 \times 22 \times 45$ was too stiff to serve the intended purpose. We also tested
370 torsion springs that did not provide a successful outcome in all angles and a
371 set of 3 tension springs that were also failed. We use $\emptyset 1.4 \times 19 \times 43$ that were
372 empirically found to be the best for our purpose and design.

373 We compared the decompression speed with and without the proposed pas-
374 sive decompression device. Table 3 shows the measured time for tested landing
375 surfaces with different angles. For each surface angle, we measured 3 times and
376 mean times are reported in the table. After turning off the power of the vac-
377 uum motor, without breaking the vacuum environment, the negative pressure

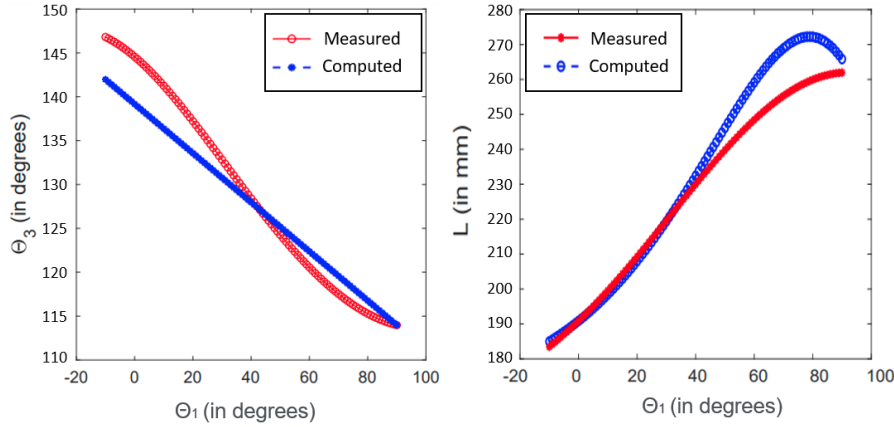


Fig. 12 These graphs denote computed values using Eqs. (1)-(6) and measured values during experiments for Θ_3 and L over Θ_1 . Small discrepancy between values are mainly the right angle assumption between legs and the surface (points A and B in Fig. 6) since this assumption does not hold always due to the universal joint.

Table 3 Pressure relief time with and without passive decompression device

$\Theta_1 = \Theta_{FL} = \Theta_{FR}$ in degrees	without device in seconds	with device in seconds
0	525	1.56
10	520	1.55
20	500	1.45
30	467	1.41
40	450	1.31
50	392	1.30
60	381	1.25
70	380	1.25
80	344	1.21
90	327	1.20
100	315	1.10

378 in the vacuum suction cup continues for a very long time, making it difficult
 379 for the UAV to leave the surface. However, when the passive decompression
 380 device is installed, as soon as the vacuum motor is turned off, the negative
 381 pressure in the suction cup is released immediately, making the UAV leave the
 382 surface quickly.

383 When robotic legs are facing front while flying, the rotation speed of the
 384 landing gear is likely to affect the stability of the UAV. We did different exper-
 385 iments with rotating speed of the servo motor. In the first experiment, when
 386 the servo motor was set to rotate 95° in 3 seconds, the UAV has lost its bal-
 387 ance and fell down. When the selected rotation time is about 5 seconds, the
 388 balance was still adversely affected, and the UAV suffered a short-term control
 389 failure. However, it did not fall down. When the selected rotation time is 10
 390 seconds, the balance was affected slightly, but it did not affect the flight.

391 In order to test the landing ability on arbitrary surfaces, we set landing
392 surface angle in view of XZ plane between $[150^\circ, 210^\circ]$ with 5-degree intervals
393 in the XZ plane simulating the cases depicted in Fig. 5. We performed 10
394 landing trials for each angle. We observed that the larger the angle, the more
395 accurate speed and angle of the UAV control are required. The UAV control
396 became very difficult when the angle is within the intervals $[150^\circ, 160^\circ]$ and
397 $[195^\circ, 210^\circ]$. For the rest of angles tested, the UAV has attached to the target
398 surface easily. According to experiments, the front leg is designed for different
399 angles and has an adaptive correction capability of about $\pm 20^\circ$ of the target
400 surface. The angle change greater than $\pm 20^\circ$ from 180° will increase the diffi-
401 culty of UAV control, therefore such condition is normally not suitable for the
402 proposed landing gear design.

403 5 Conclusions and Future Work

404 Over the last decade, an increasing number of studies have attempted to design
405 various types of UAVs flying autonomously outfitted with different sensors and
406 enable them to maintain stable contact with the environment for remote in-
407 spection and monitoring. Along the lines, this paper presented a novel robotic
408 landing gear with 3 angle-adjustable robotic legs helping UAVs stick to the
409 structure surface by a vacuum system. In the proposed design, the robotic
410 landing gear allows the UAV to land on irregular surfaces. A passive angle
411 adjustment method was adopted based on the mechanical structure to effec-
412 tively reduce weight and power consumption. It was demonstrated through our
413 laboratory experiments that this design can be easily connected to irregular
414 surfaces such as uneven and curved surfaces.

415 For future work, we will aim at developing a cooperative flight control
416 system with the robotic landing gear, allowing the robotic landing gear and
417 surface contact interaction to transition in a more stable and safer way before
418 and after connecting to the terrain.

419 **Acknowledgements** This material is based upon work supported by the U.S. Air Force
420 Office of Scientific Research under AFOSR/AOARD FA2386-20-1-4019 grant.

421 References

- 422 1. Albers, A., Trautmann, S., Howard, T., Nguyen, T.A., Frietsch, M., Sauter, C.: Semi-
423 autonomous flying robot for physical interaction with environment. In: 2010 IEEE
424 Conference on Robotics, Automation and Mechatronics, pp. 441–446. IEEE (2010)
- 425 2. Bass, J., Desbiens, A.L.: Improving multirotor landing performance on inclined surfaces
426 using reverse thrust. *IEEE Robotics and Automation Letters* **5**(4), 5850–5857 (2020).
427 DOI 10.1109/LRA.2020.3010208
- 428 3. Bisht, R.S., Alexander, S.J.: Mobile robots for periodic maintenance and inspection of
429 civil infrastructure: a review. In: International Conference on Machines and Mechanisms,
430 pp. 1050–1057 (2013)
- 431 4. Dethe, R.D., Jaju, S.: Developments in wall climbing robots: a review. *International*
432 *journal of engineering research and general science* **2**(3), p33–42 (2014)

- 433 5. Gago, J., Douthe, C., Coopman, R., Gallego, P., Ribas-Carbo, M., Flexas, J., Escalona,
434 J., Medrano, H.: Uavs challenge to assess water stress for sustainable agriculture. *Agricul-*
435 *tural water management* **153**, 9–19 (2015)
- 436 6. Gómez-Candón, D., De Castro, A., López-Granados, F.: Assessing the accuracy of mo-
437 saics from unmanned aerial vehicle (uav) imagery for precision agriculture purposes in
438 wheat. *Precision Agriculture* **15**(1), 44–56 (2014)
- 439 7. González-deSantos, L.M., Martínez-Sánchez, J., González-Jorge, H., Arias, P.: Active
440 uav payload based on horizontal propellers for contact inspections tasks. *Measurement*
441 **165**, 108106 (2020)
- 442 8. Hallermann, N., Morgenthal, G.: Visual inspection strategies for large bridges using
443 unmanned aerial vehicles (uav). In: *Proc. of 7th IABMAS, International Conference on*
444 *Bridge Maintenance, Safety and Management*, pp. 661–667 (2014)
- 445 9. Ichikawa, A., Abe, Y., Ikeda, T., Ohara, K., Kishikawa, J., Ashizawa, S., Oomichi,
446 T., Okino, A., Fukuda, T.: Uav with manipulator for bridge inspection—hammering
447 system for mounting to uav. In: *2017 IEEE/SICE International Symposium on System*
448 *Integration (SII)*, pp. 775–780. IEEE (2017)
- 449 10. Ikeda, T., Yasui, S., Fujihara, M., Ohara, K., Ashizawa, S., Ichikawa, A., Okino, A.,
450 Oomichi, T., Fukuda, T.: Wall contact by octo-rotor uav with one dof manipulator for
451 bridge inspection. In: *2017 IEEE/RSJ International Conference on Intelligent Robots*
452 *and Systems (IROS)*, pp. 5122–5127. IEEE (2017)
- 453 11. Iwamoto, T., Enaka, T., Tada, K.: Development of testing machine for tunnel inspection
454 using multi-rotor uav. In: *Journal of Physics: Conference Series*, vol. 842, p. 012068.
455 IOP Publishing (2017)
- 456 12. Jarman, M., Vesey, J., Febvre, P.: Unmanned aerial vehicles (uavs) for uk agriculture:
457 *Creating an invisible precision farming technology. White Paper, July* (2016)
- 458 13. Jimenez-Cano, A., Heredia, G., Ollero, A.: Aerial manipulator with a compliant arm
459 for bridge inspection. In: *2017 International Conference on Unmanned Aircraft Systems*
460 *(ICUAS)*, pp. 1217–1222. IEEE (2017)
- 461 14. Jung, S., Shin, J.U., Myeong, W., Myung, H.: Mechanism and system design of mav
462 (micro aerial vehicle)-type wall-climbing robot for inspection of wind blades and non-flat
463 surfaces. In: *2015 15th International Conference on Control, Automation and Systems*
464 *(ICCAS)*, pp. 1757–1761. IEEE (2015)
- 465 15. Kamel, M., Verling, S., Elkhatib, O., Sprecher, C., Wulkop, P., Taylor, Z., Siegwart,
466 R., Gilitschenski, I.: Voliro: An omnidirectional hexacopter with tiltable rotors. *arXiv*
467 *preprint arXiv:1801.04581* (2018)
- 468 16. Mahmood, S., Bakhy, S., Tawfik, M.: Propeller-type wall-climbing robots: A review. In:
469 *IOP Conference Series: Materials Science and Engineering*, vol. 1094, p. 012106. IOP
470 Publishing (2021)
- 471 17. Myeong, W., Jung, S., Yu, B., Chris, T., Song, S., Myung, H.: Development of wall-
472 climbing unmanned aerial vehicle system for micro-inspection of bridges. In: *2019 In-*
473 *ternational Conference on Robotics and Automation (ICRA)*. IEEE (2019)
- 474 18. Myeong, W., Myung, H.: Development of a wall-climbing drone capable of vertical soft
475 landing using a tilt-rotor mechanism. *IEEE Access* **7**, 4868–4879 (2018)
- 476 19. Myeong, W.C., Jung, K.Y., Jung, S.W., Jung, Y., Myung, H.: Development of a drone-
477 type wall-sticking and climbing robot. In: *2015 12th International Conference on Ubiq-*
478 *uitous Robots and Ambient Intelligence (URAI)*, pp. 386–389. IEEE (2015)
- 479 20. Paul, H., Miyazaki, R., Ladig, R., Shimonomura, K.: Landing of a multirotor aerial
480 vehicle on an uneven surface using multiple on-board manipulators. In: *2019 IEEE/RSJ*
481 *International Conference on Intelligent Robots and Systems (IROS)*, pp. 1926–1933.
482 IEEE (2019)
- 483 21. Pope, M.T., Kimes, C.W., Jiang, H., Hawkes, E.W., Estrada, M.A., Kerst, C.F., Rod-
484 erick, W.R., Han, A.K., Christensen, D.L., Cutkosky, M.R.: A multimodal robot for
485 perching and climbing on vertical outdoor surfaces. *IEEE Transactions on Robotics*
486 **33**(1), 38–48 (2016)
- 487 22. Ratsamee, P., Kriengkamol, P., Arai, T., Kamiyama, K., Mae, Y., Kiyokawa, K.,
488 Mashita, T., Uranishi, Y., Takemura, H.: A hybrid flying and walking robot for steel
489 bridge inspection. In: *2016 IEEE International Symposium on Safety, Security, and*
490 *Rescue Robotics (SSRR)*, pp. 62–67. IEEE (2016)

-
- 491 23. Ridao, P., Carreras, M., Ribas, D., Garcia, R.: Visual inspection of hydroelectric dams
492 using an autonomous underwater vehicle. *Journal of Field Robotics* **27**(6), 759–778
493 (2010)
- 494 24. Sanchez-Cuevas, P.J., Ramon-Soria, P., Arrue, B., Ollero, A., Heredia, G.: Robotic
495 system for inspection by contact of bridge beams using uavs. *Sensors* **19**(2), 305 (2019)
- 496 25. Song, Y.K., Lee, C.M., Koo, I.M., Tran, D.T., Moon, H., Choi, H.R.: Development of
497 wall climbing robotic system for inspection purpose. In: 2008 IEEE/RSJ International
498 Conference on Intelligent Robots and Systems, pp. 1990–1995. IEEE (2008)
- 499 26. Tsukagoshi, H., Watanabe, M., Hamada, T., Ashlih, D., Iizuka, R.: Aerial manipulator
500 with perching and door-opening capability. In: 2015 IEEE International Conference on
501 Robotics and Automation (ICRA), pp. 4663–4668. IEEE (2015)
- 502 27. Watanabe, K., Nakatsuka, T., Nagai, I.: Production of a wall-climbing-type quadrotor
503 and its experiment for verifying basic operations. In: 2018 IEEE International Confer-
504 ence on Mechatronics and Automation (ICMA), pp. 1850–1855. IEEE (2018)